RESEARCH ARTICLE

Importance of DA-MRF Models in Fuzzy Based Classifier

**Mrinal Singha · Anil Kumar · Alfred Stein ·
P. N. L. Raju · Y. V. N. Krishna Murthy**

Abstract This research considers the smoothness prior and four discontinuity adaptive Markov Random Field (DA-MRF) models to deal with discontinuity adaptation for the contextual fuzzy c-means (FCM) classifier. They were applied to classify AWiFS and LISS-III images from the Resourcesat-1 and Resourcesat-2 satellites. A fraction image from the high resolution LISS-IV image has been used as reference data. Quality of the classified AWiFS and LISS-III images was assessed by means of an image to image fuzzy error matrix (FERM). The classification accuracy increased by 1.5 to 6 % as compared to the conventional FCM. Classification accuracy increased with 0.5 to 8 % when comparing Resourcesat-2 with Resourcesat-1 data. The study showed that DA3-MRF model with FCM performed better than other MRF models, showing an improved overall classification accuracy as well as preserving the edges at boundaries.

Introduction

Pixels of satellite images represent reflection values of land cover classes. The pixels can either be pure, representing a single land cover class, or mixed, representing a combination of land cover classes. The majority of the pixels are of a mixed type, due to gradual changes of real world phenomena,

M. Singha · A. Kumar (✉) · P. N. L. Raju · Y. V. N. K. Murthy
Indian Institute of Remote Sensing, Dehradun, India
e-mail: anil@iirs.gov.in

A. Stein
Geo-Information Science and Earth Observation of the University of Twente, Enschede, The Netherlands
e-mail: a.stein@utwente.nl

boundaries between classes that do not match with pixel geometry and the restricted spatial resolution that is unable to capture such variation. In standard classification techniques, however, it is assumed that pixels are pure. For this reason Zhang and Foody (2001) proposed to adapt fuzziness in the classification procedures so that individual pixels may level with multiple and partial class memberships. Fuzzy c-means clustering (FCM) is widely used for this purpose (Bezdek et al. 1984). FCM classifies mixed pixels by assigning membership grades to individual classes, but in a default setting it does not consider spatial contextual information. The spatial context of a pixel is the presence of similar class labels at neighboring pixels (Solberg et al. 1996). Isolated pixels, i.e. pixels with values that are entirely different from values at the neighboring positions rarely exist. Context may be useful in classification procedures as it may help to properly deal with the combination of isolated pixels and mixed pixels (Tso and Mather 2009). The aim of contextual information is to reduce noise present in remote sensing data, where noise may be due to the sensor or to areas of classes that are smaller than areas that are to be represented at the desired land use/land cover map scale.

Various studies have been conducted related to spatial contextual information with various classification algorithms to improve image classification and segmentation such as adaptive Bayesian contextual classification (Jackson and Landgrebe 2002), multisource classification (Solberg et al. 1996) and multisource classification with a genetic algorithm (Tso and Mather 1999). Xu and Ohya (2010) found that FCM can improve the image segmentation accuracy even in the presence of noise, if it is made context sensitive. Pham penalized the FCM objective function for the behavior of membership functions while incorporating spatial information and observed improved segmented result in the presence of noise (Pham 2001). Spatial contextual information in classification methods can be incorporated in different ways. A relatively

straight forward method is to use majority voting within a prescribed window where the central pixel is replaced with the class that most often occurs (Tso and Olsen 2005). A more advanced way is to incorporate spatial contextual information by means of Markov Random Fields (MRF) (Geman and Geman 1984; Solberg et al. 1996; Amador 2005; Li 2009; Moser and Serpico 2010). A common assumption in MRF modeling is that of uniform smoothness, which implies the same degree of smoothness over a full image. Leaving discontinuities out of consideration, however, leads to over smoothed, less accurate and hence undesirable results (Li 2009 and 1995). Discontinuity adaptive (DA) MRF (Li 1995) models or adaptive neighborhood (Debayle and Pinoli 2006) can be used to overcome such problems of discontinuity. So far, contextual based information of an image has not been combined with fuzzy based spectral classifiers.

The aim of this study was to combine discontinuity adaptive (DA) MRF models with spatial contextual information within a FCM classifier. DA-MRF models focused both on smoothing the classified output and on edge preservation of class boundaries. The accuracy of the classified output has been assessed using the fuzzy error matrix (FERM) (Binaghi et al. 1999) and the uncertainty was evaluated using the entropy method (Dehghan and Ghassemian 2006).

Classification and Accuracy Approaches

Fuzzy c-Means Approach (FCM)

Fuzzy c-means (FCM) classification, introduced by Bezdek et al. (1984), calculates the membership values of the each pixel to different classes. It is based on finding the membership values μ_{ij} of the ith pixel for class j^{th} that minimize the objective function as mentioned in Eq. (1);

$$J_m(U,V) = \sum_{j=1}^{N} \sum_{i=1}^{C} \mu_{ij}^m d_{ij}^2, \quad 1 \le m < \infty. \tag{1}$$

Here, N is the total number of the pixels, c is the number of classes, μ_{ij} is the membership value of the ith pixel for class j, m is a weighing exponent and d_{ij} is the (Euclidean) distance between unknown feature vector X_i and the mean feature vector V_j of class j. Optimization is done by means of an iterative procedure between Eqs. (2) and (3) on the membership values and the cluster centers (Dulyakarn and Rangsanseri 2001):

$$\mu_{ij} = \frac{1}{\sum\limits_{k=1}^{c} \left(\frac{d_{ij}}{d_{ik}}\right)^{\frac{2}{m-1}}} \tag{2}$$

$$V_i = \frac{\sum\limits_{j=1}^{n} \mu_{ij}^m X_j}{\sum\limits_{j=1}^{n} \mu_{ij}^m} \tag{3}$$

After an initial choice for class means, e.g. on the basis of a hard classification, class means are estimated, that result into new membership values, which in turn can lead to new class means. This procedure is repeated until convergence occurs.

Integrating the FCM with MRF

The objective function of FCM with MRF incorporates spatial contextual information using smoothness prior and DA-MRF models (Li 2009). The objective function of FCM with MRF is similar to the objective function of FCM to which neighbourhood information is included. Objective function (4) has been formulated using smoothness prior and from now onwards it will be referred to as FCM-S.

$$U\left(\mu_{ij}|d\right) = (1-\lambda)\left[\sum_{i=1}^{N}\sum_{j=1}^{C}\mu_{ij}^m d_{ij}^2\right] \\ + \left[\sum_{i=1}^{N}\sum_{j=1}^{C}\sum_{j'\in N_i}\beta\left(\mu_{ij}-\mu_{ij'}\right)^2\right] \tag{4}$$

where $U(\mu_{ij}|d)$ is the Global Posterior energy of membership value μ_{ij} for given image data, λ with $0 <\lambda<1$ is the smoothness strength, i.e. the weight between spectral and contextual information, $\beta> 0$ is the weight for neighbors and N_i is the neighborhood window around pixel i. In Eq. (4) spectral information has been included by using the objective function of FCM. In this way, the conditional energy and spatial contextual information is incorporated by using the smoothness prior as prior energy has been introduced.

Next, objective functions are formulated using discontinuity adaptive (DA) MRF models. Let η be defined as $\eta = (\mu_{ij}-\mu_{ij})$ i.e. the difference between the membership value of the target pixel (pixel i) and the membership value of a neighboring pixel in neighborhood N_i. Then $U(\mu_{ij}|d)$ objective function will be as in Eqs. (5) to (8);

$$U\left(\mu_{ij}|d\right) = (1-\lambda)\left[\sum_{i=1}^{N}\sum_{j=1}^{C}\mu_{ij}^m d_{ij}^2\right] \\ + \lambda\left[\sum_{i=1}^{N}\sum_{j=1}^{C}\sum_{j'\in N_i}\left(-\gamma e^{-\frac{\eta^2}{\gamma}}\right)\right] \tag{5}$$

$$U\left(\mu_{ij}\middle|d\right) = (1-\lambda)\left[\sum_{i=1}^{N}\sum_{j=1}^{C}\mu_{ij}^{m}d_{ij}^{2}\right] \qquad (6)$$
$$+ \lambda\left[\sum_{i=1}^{N}\sum_{j=1}^{C}\sum_{j'\in N_{i}}\left(-\frac{\gamma}{1+\frac{\eta^{2}}{\gamma}}\right)\right]$$

$$U\left(\mu_{ij}\middle|d\right) = (1-\lambda)\left[\sum_{i=1}^{N}\sum_{j=1}^{C}\mu_{ij}^{m}d_{ij}^{2}\right] \qquad (7)$$
$$+ \lambda\left[\sum_{i=1}^{N}\sum_{j=1}^{C}\sum_{j'\in N_{i}}\gamma\ln\left(1+\frac{\eta^{2}}{\gamma}\right)\right]$$

$$U\left(\mu_{ij}\middle|d\right) = (1-\lambda)\left[\sum_{i=1}^{N}\sum_{j=1}^{C}\mu_{ij}^{m}d_{ij}^{2}\right]$$
$$+ \lambda\left[\sum_{i=1}^{N}\sum_{j=1}^{C}\sum_{j'\in N_{i}}\left(\gamma|\eta|-\gamma^{2}\ln\left(1+\frac{|\eta|}{\gamma}\right)\right)\right] \qquad (8)$$

where γ, with $0 <\gamma< 1$, controls the interaction between the two pixels (Li 2009). Equations (5)–(8) will be referred to as FCM DA1, FCM DA2, FCM DA3 and FCM DA4, respectively.

Edge Verification

In this research work, attention focuses on classified outputs of grey level fraction images. For a grey level image an edge represents the boundaries between the two classes. An edge can be characterized as a step function or slop between two regions (Wen and Xia 1999). Let μ_1 and μ_2 be the mean value of the grey levels on either side of an edge. Following (Wen and Xia 1999), there is no significant difference between the grey levels on the two sides of the edge, if for a well-specified threshold c, $|\mu_1-\mu_2|\leq c$, whereas if $|\mu_1-\mu_2|>c$, a significant difference occurs. To verify the edges, it have been considered fraction images that are output images for each class representing membership values, as degree of belongingness of each pixel to each class. A homogeneous area was selected for each class from the classified fraction image with a high mean membership value and a low variance. Classes in the study area are Eucalyptus Plantation, Dry agriculture field without crop and Water. Such selections are relatively homogeneous, because of their high membership values and low variances. Next, two sets of pixels were selected at either side of the edge. The pixels belonging to the first set have a high mean value to a particular class, as these pixels all have a high membership values to this class, where as pixels at the other side of the edge do not belong to that class and thus this set has

a low mean membership value. Contextual information further reduces noise within classes and therefore homogeneity within class increases and the variance within the class will be reduced further. The mean difference of these two sets of pixels hence will be high and the variance low if the edge is preserved.

Accuracy of Classification

To measure the accuracy of the soft classified output, the Fuzzy Error Matrix (FERM) (Binaghi et al. 1999) was used. The FERM derives the accuracy of a fuzzy classification output from the fraction images. FERM is used the same as the traditional error matrix, except that elements of a fuzzy error matrix can be non-negative real numbers as compared to non-negative integer numbers used in a conventional error matrix.

Entropy as a measure of absolute uncertainty (Dehghan and Ghassemian 2006) is an indirect method of accuracy assessment that does not take any reference data to a particular measure of uncertainty. Entropy can be used as an accuracy measure in the absence of reference data. The entropy is expressed as in Eq. (9);

$$Entropy(x) = \sum_{i=1}^{C}-\mu_{ij}\log_{2}\mu_{ij} \qquad (9)$$

Where c denotes total number of classes and μ_{ij} is the estimated membership function.

A high uncertainty corresponds with a high entropy value and vice versa. In this way visualization of entropy can reflect uncertainty of a classification. In this study the entropy was used to optimize the parameters involved in FCM-S and FCM DA-MRF models, by evaluating the uncertainty in the classified output.

Study Area and Data Used

The study area selected for this research work was the Sitarganj Tehsil area located near Pant Nagar within Uttarakhand state, India. The area extends from 28°53′57″N to 28°56′31″N latitude and from 79°34′22″E to 79°36′35″E longitude. The study area presents different land cover classes like Sal forest, Eucalyptus plantation, agricultural land with sugarcane and paddy as major crops and two water reservoirs namely, the Baigul reservoir and the Dhora reservoir (Fig. 1).

Remote sensing images used for this study were obtained by means of the LISS-IV, LISS-III and AWiFS sensors of ResourseSat-1 and 2 satellites. AWiFS and LISS-III are four band data and LISS-IV is three band data. One of the reasons to select this study area was that LISS-IV, LISS-III and AWiFS images were acquired at the same dates. All the six images

Fig. 1 Location of study area from Reseourcesat-2 LISS-III images
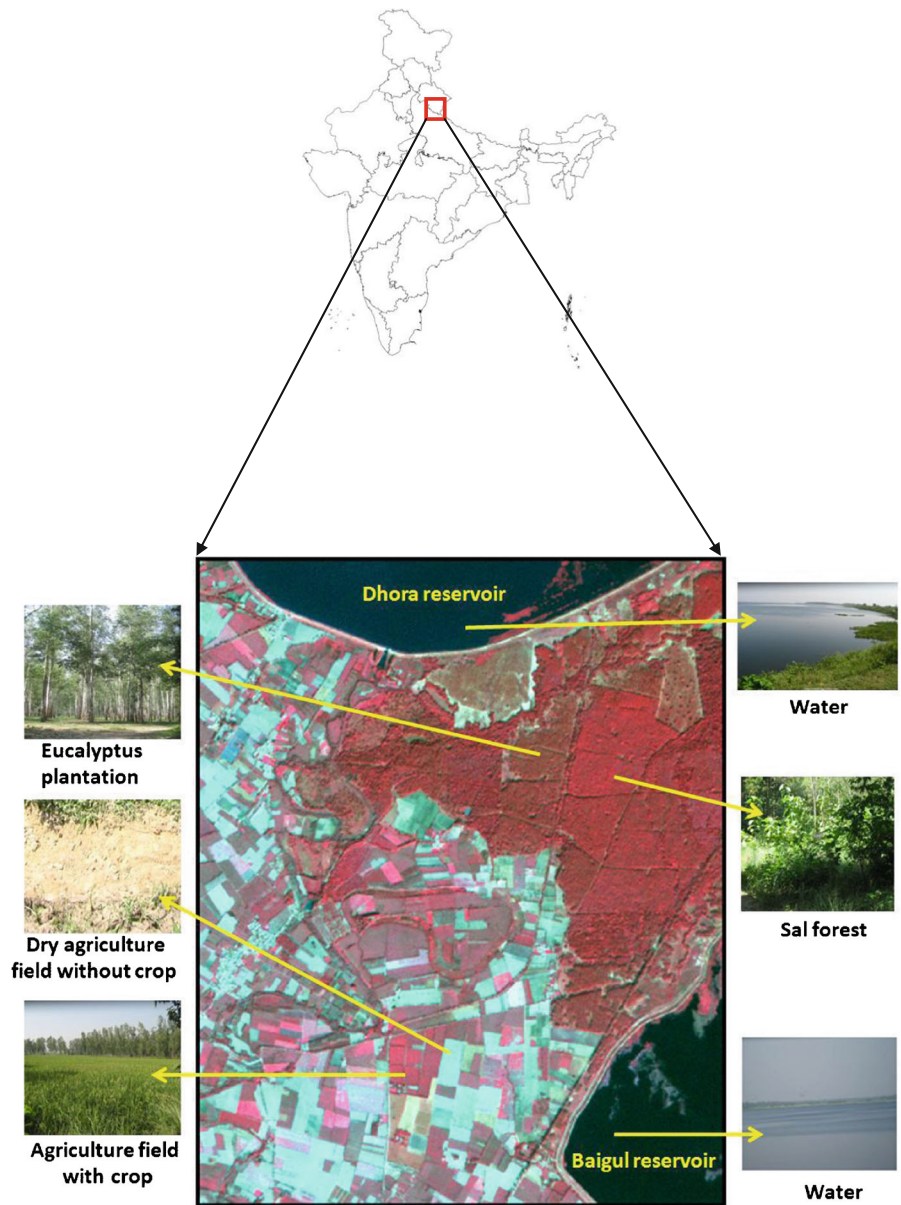
Fig. 2 Adopted methodology
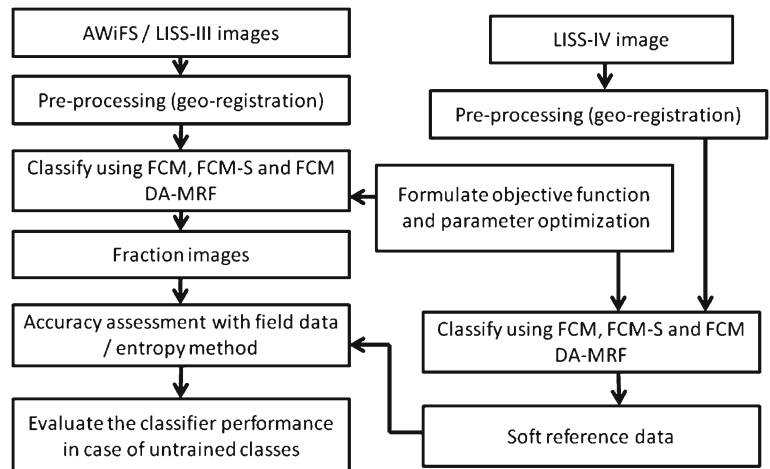
(LISS-IV, LISS-III and AWiFS) were geometrically corrected and resampled using nearest neighbour resample method to 5, 20 and 60 m spatial resolution respectively. LISS-III and AWiFS have been used to generate soft classified output from ResourseSat-1 and ResourseSat-2 satellites respectively, where as the classified LISS-IV images have been used as reference data. In doing so, the number of LISS-IV pixels corresponded with the number of LISS-III and AWiFS pixels (here, 16 pixels for LISS-III and 144 pixels for AWiFS), which was convenient for image to image accuracy assessment.

Implementation

Implementation of the methodology is given in Fig. 2. A training dataset was collected from the AWiFS, LISS-III and LISS-IV images on the basis of ground field visit information. In total, c=6 and c=5 land cover classes were selected for the images from Resourcesat-1 and Resourcesat-2, respectively. Considered land cover classes were c_1 = agriculture field with crop, c_2 = eucalyptus plantation, c_3 = dry agriculture field without crop, c_4 = moist agriculture field without crop, c_5 = sal forest and c_6 = water. For Resourcesat-2 images, c_4 was not considered. In total 50 and 60 training pixels were selected for Resourcesat-1 and Resourcesat-2, respectively, following the $10n$ rule for sampling (Jensen 1996) to train the classifiers, where n is number of bands. According to Congalton (1991), 100 pixels were randomly selected within each class from both the classified and reference images for accuracy assessment.

After preprocessing and training dataset preparation, the AWiFS, LISS-III and LISS-IV images were classified separately by FCM, FCM-S and FCM DA1—FCM DA4 classifiers. For the FCM-S and FCM DA classifiers, parameters λ, β and γ were optimized using entropy values while considering that edges were preserved using mean difference and variance as explained in Edge Verification. Several experiments were performed to estimate the parameters λ, β and γ. Entropy values and edge verification were checked following a range from 0.1 to 0.9 for λ and from 1 to 9 for β. Similarly λ and γ

Table 2 Overall accuracy obtained by the five different classifiers for AWiFS image from Resourcesat-1 and Resourcesat-2

Classifiers	Recourcesat-1 (%)	Resourcesat-2 (%)
FCM-S	76.04	84.75
FCM DA1	79.84	82.37
FCM DA2	76.25	82.87
FCM DA3	81.97	87.02
FCM DA4	81.71	82.94

were estimated taking the range of γ from 0.1 to 0.9. Optimized values of these values have been mentioned in Table 1. After estimating the parameters, the AWiFS and LISS-III images were classified with the optimized parameter values and the fuzzy accuracy was measured using FERM.

The optimized output fraction images of AWiFS and LISS-III were validated while applying developed contextual based classifier with respect to the soft reference dataset generated from LISS-IV data. A JAVA based tool developed by Kumar et al. (2006) has been used for accuracy assessment in this research work. The performance of contextual based classifiers was tested with respect to untrained classes present in the study area. The untrained class means, a class is present on the ground but not considered for classification. That means while testing classified outputs, classified output were generated while not considering untrained class but reference data was generated while considering untrained class also.

Results

The optimized parameter values for all the classifiers have been presented in Table 1. Values for λ and β for the FCM-S classifier are in the range of 0.7–0.9 and 2 respectively. The λ and γ values for FCM DA classifiers are in the range of 0.7–0.9 and 0.2–0.5 respectively. There was a 5.85 % increase in the overall classification accuracy of contextual FCM DA3 as compared to the FCM classifier for AWiFS Resourcesat-1 image, whereas there was a 1.61 % increase in the overall accuracy of contextual FCM DA3 as compared to the FCM classifier for LISS-III Resourcesat-1 image, as shown in

Table 1 Optimized parameter values for the five different classifiers applied to three different sensors of Resourcesat-1 and Resourcesat-2

Classifiers and parameters	AWiFS	LISS-III	LISS-IV
FCM-S (λ/β)	0.9/2	0.9/2	0.7/2
FCM DAI (λ/γ)	0.7/0.2	0.7/0.2	0.7/0.2
FCM DA2 (λ/γ)	0.9/0.4	0.9/0.4	0.9/0.3
FCM DA3 (λ/γ)	0.9/0.2	0.9/0.2	0.6/0.2
FCM DA4 (λ/γ)	0.9/0.5	0.9/0.5	0.8/0.4

Table 3 Overall accuracy obtained by different classifiers for the LISS-III image from the Resourcesat-1 and Resourcesat-2 satellites

Classifiers	Recourcesat-1 (%)	Resourcesat-2 (%)
FCM-S	85.72	86.22
FCM DA1	84.96	83.86
FCM DA2	83.9	83.76
FCM DA3	87.31	87.85
FCM DA4	85.0	85.29

Table 4 Verification of edge preservation for the AWiFS and LISS-III images at the Resourcesat-1 satellite

Class	AWiFS				LISS-III			
	FCM-S		FCM DA3		FCM-S		FCM DA3	
	Difference in mean	Variance	Difference in mean	Variance	Difference in mean	Variance	Difference in mean	Variance
Eucalyptus Plantation	153.5	1104.5, 2	157	1104.5, 0.5	216.5	4.5, 2	229.5	4.5, 2
Water	240	4.5, 40.5	247	4.5, 18	231.5	8, 4.5	239.5	2, 4.5

Table 2. There was a 5.0 % increase in overall classification accuracy of contextual FCM DA3 as compared to the FCM classifier for the AWiFS Resoursesat-2 image, whereas there was a 3.0 % increase in overall accuracy of the contextual FCM DA3 as compared to the FCM classifier for the LISS-III Resoursesat-2 image, as shown in Table 3. In Tables 2 and 3 the overall classification accuracy for the FCM, FCM-S and FCM DA classifiers have been provided for both the AWiFS and LISS-III images from the Resourcesat-1 and Resourcesat-2 satellites. From Tables 2 and 3 it is clear that FCM DA3 classifier performed better than the other classifiers studied in this research work.

As in Tables 4 and 5 the edge verification was conducted using mean and variance method for three land cover classes i.e. Eucalyptus plantation, dry agriculture field without crop and water. These 3 classes out of the 6 original classes were considered for edge verification because water is a relatively homogenous class, where as Eucalyptus plantation and dry agriculture field without crops show heterogeneous within class variation. As compared to FCM and FCM-S the FCM DA3 best preserves the class edges. This has been concluded based on mean difference is higher and variance was lowest from Tables 4 and 5.

The performance of the developed contextual classifier was evaluated as well for untrained classes. To obtain untrained classes, the mean value for a known class was not provided during training of the classifier and the classification was performed with the remaining classes (Foody 2000). The performance of the FCM-S classifier was tested for untrained classes when class 2 i.e. agriculture field with crop, selected at random, was not considered. The fuzzy user's accuracy has decreased with 9.17 %, if this untrained class was absent during the FCM-S classification. This means that the accuracy for each class on the classified output has decreased as compared to the reference classes. Similarly the performance of FCM DA has been checked for the untrained classes. For this purpose the FCM DA3 classifier is taken where class 2 i.e. agriculture field with crop retained untrained. Similar to the FCM-S classifier, the fuzzy user's accuracy decreased with 4.46 % if class 2 had been untrained in FCM DA classification. This concludes that the FCM DA3 has been least affected if an untrained class was absent.

In Fig. 3 the average user's accuracy has been compared for different classifiers with and without untrained class. In the presence of untrained class the user's accuracy decreased with 10.63, 9.17, and 4.46 % for FCM, FCM-S and FCM DA3, respectively. Similar results were observed for untrained class for the Resourcesat-2 AWiFS and the LISS-III images. As concerns edge preservations it has been observed from Fig. 4 that FCM DA3 preserves the edges present on the input image, where as edges were not preserved when applying the FCM-S classifier.

Discussion

This research presents context based image classification that uses the smoothing MRF model as well as discontinuity adaptive MRF models. The smoothness parameter (λ) for the MRF models changes across the spatial resolution of

Table 5 Verification of edge preservation for the AWiFS and LISS-III images at the Resourcesat-2 satellite

Class	AWiFS				LISS-III			
	FCM-S		FCM DA3		FCM-S		FCM DA3	
	Difference in mean	Variance	Difference in mean	Variance	Difference in mean	Variance	Difference in mean	Variance
Dry agriculture field without crop	243.8	27.5, 2.2	247.2	37.5, 0.2	242	8, 0.5	247.5	8, 0.5
Water	223.5	882, 0.5	244	0.5, 4.5	224.5	264.5, 2	239	0.5, 0.5

Fig. 3 Comparison of average
user's accuracy of different
classifiers for LISS-III image
from Resourcesat-1. **a** Input
image **b** FCM-S **c** FCM DA-
MRF (H3)

Performance of classifiers on trained and untrained classes
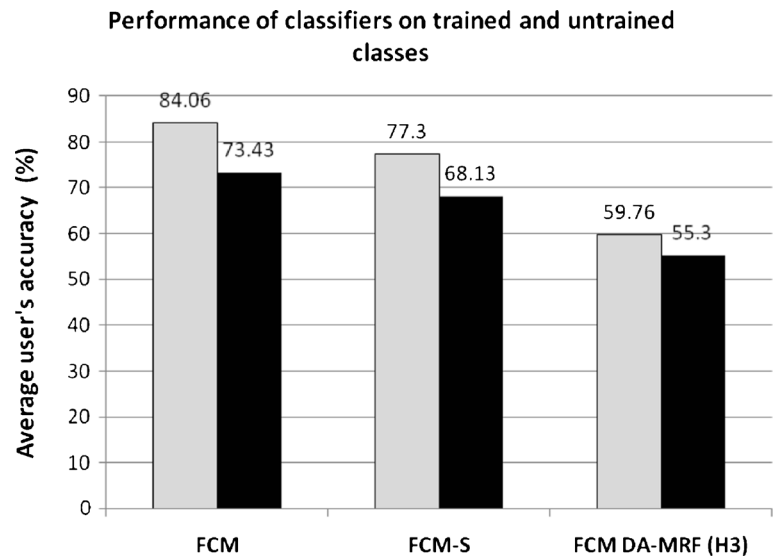
images. For coarser resolution image the value of λ was higher, because of the low variability in the image, where as for fine resolution image it was lower. Further, the optimum λ value for an image remains the same irrespective of the radiometric accuracy of an image. The radiometric accuracy improved from 7 bits to 10 bits for LISS-III and LISS-IV and 10 bits to 12 bits for AWiFS in Resourcesat-2 as compared to Resourcesat-1. For both the Resourcesat-1 and Resourcesat-2 the estimated parameter value of λ and γ were found to have similar values. The FCM classifier only takes spectral properties for classification but due to incorporation of spatial contextual information it also consider the spatial properties of the image and it increases the overall classification accuracy.

To combine contextual spatial information with FCM, smoothness prior and four DA-MRF models have been used. The increase of the overall accuracy upon using DA-MRF models as compared to the smoothness prior was due to the interactions among the pixels. Those were assumed to be constant in the smoothness prior model, where as its smoothing strength was set proportional to a function of $|\eta|$ in the DA-MRF models. The FCM-S classifier, therefore, results in over-smoothing at the edges where it crosses boundaries. For

that reason, the FCM-S classifier does not increase the classification accuracy.

The developed classifier was tested both on Resourcesat-1 and Resourcesat-2 images. Apart from the improvement in the classification accuracy, the radiometric accuracy also affected the visual appearance of the classified output. For the Resourcesat-2 image, the land cover classes were more clearly visible and well separated from other classes as compared to the Resourcesat-1 image.

To study the preservation of edges for classified output, mean and variance method has been used, where edges were checked on a pixel wise basis for the classified AWiFS and LISS-III images. As confirmed in (Li 2009) the DA-MRF models preserve the edges whereas smoothness prior leads to over smoothing. The results obtained by edge verification show that the DA-MRF models preserved the edges better with the high mean difference and low variance than the smoothness prior. This was due to DA-MRF models in smoothing strength was set proportional to a function of $|\eta|$ in the DA-MRF models.

The preservation of edge has been checked for all the classifiers using mean and variance method for AWiFS and

Fig. 4 Effects of contextual
classification on the edges

Input image   FCM-S   FCM DA-MRF (H3)
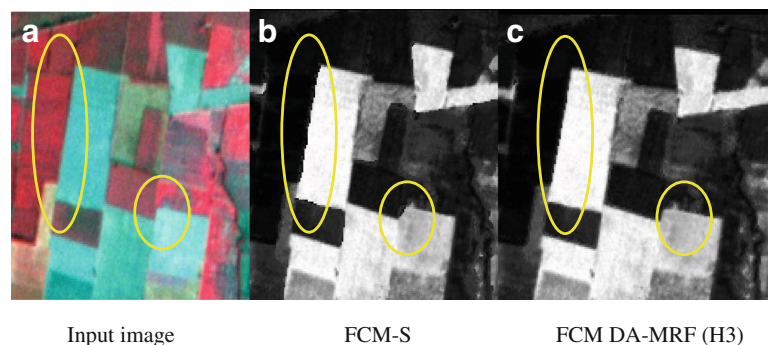
LISS-III images. The FCM DA classifiers, preserves the edges better whereas FCM-S was unable to preserve the edges. This was due to interactions among the pixels to be constant in the smoothness prior model but for the FCM DA classifiers the smoothing strength was set proportional to a function of $|\eta|$. Preserving the edges, moreover, improved the classification accuracy with 1.5 to 6 % for FCM DA3 as compared to FCM-S. It concludes that while using contextual classification it is important to preserve the edges and hence to avoid oversmoothing of the classified output. Upon comparing FCM-S and FCM DA-MRF it was found that FCM DA3 provides the highest classification accuracy for both the AWiFS and LISS-III images because of the following two reasons:

- In FCM DA3, η is the difference between target pixel membership value and its neighboring pixels membership value in a neighborhood window. This DA model allows a monotonic increase of the smoothing strength as η increases within the neighborhood window. Outside the window, the smoothing strength decreases as η increases and becomes zero as $\eta \to \infty$, whereas in FCM-S, it allows boundless smoothing when $\eta \to \infty$ (Li 2009).
- At homogeneous classes, where $\eta = 0$, the FCM DA3 applies zero smoothing and it controls the over smoothing

The FCM-DA1, the FCM-DA2 and the FCM-DA3 models behave in a similar way with respect to the smoothness prior model when $\frac{\eta^2}{\gamma} \ll 1$ or $\eta^2 \ll 1$ as mentioned in Li (1990). A power series expansion of $g_\gamma(\eta)$ in Eqs. (5)–(7), confirms that the DA-MRF models in (5)–(7) behave a similar way as a smoothness prior model, if the term η^2/γ is sufficiently small. Therefore, the FCM DA4 classifier also provides a classification accuracy that is close to that obtained by the FCM DA3 classifier as the adjustment function applied in the first, is similar to that applied in the latter.

The developed contextual classifier was tested as well for untrained classes. In their presence the accuracy of classified output decreased significantly for all the DA-MRF classifiers. The FCM, FCM-S and the FCM DA3 have been tested and their results were compared for untrained class. It has been found that the FCM DA3 was least affected by presence of untrained classes in comparison to FCM and FCM-S. This indicates FCM DA3 classifier is least dependent upon other classes present in the area.

Conclusions

In this research work spatial contextual information has been added to FCM classification using the smoothness MRF model and the discontinuity adaptive MRF models to generate

edge preserved fraction outputs. It can be concluded from the optimized value of λ for LISS-IV and LISS-III images, equal to 0.6 and 0.9, respectively, that the contribution of spatial contextual information was lower for a coarse resolution image than for a fine resolution image.

Further, from the results of accuracy assessment for AWiFS and LISS-III images, it can be concluded that the FCM-S and FCM DA classifiers perform better for the LISS-III image than the FCM does for the AWiFS image. If the spatial resolution of the image becomes finer, the effects of the spatial context increase. Using a DA-MRF model resulted in a further improvement of the accuracy and edge preservation for the LISS-III image as compared to AWiFS image. Therefore, the effects of discontinuities increase and edge preservation become more prominent, if spatial resolution becomes finer. The FCM DA3 classifier performs best in case of coarse and moderate resolution images among all other DA-MRF models. It also preserves the discontinuities for the coarse and moderate spatial resolution image. Finally, upon comparing Resourcesat-1 with Resourcesat-2, the contextual classification accuracy increased by 0.5 to 8 %. From this research work it can therefore be concluded that the FCM DA classifiers were least affected by the presence of untrained classes as comparison to FCM-S and FCM.

References

Amador, J. J. (2005). Markov random field approach to region extraction using Tabu Search. *Journal of Visual Communication and Image Representation, 16*, 134–158.

Bezdek, J. C., Ehrlich, R., & Full, W. (1984). FCM: the fuzzy c-means clustering alogorithm. *Computers and Geosciences, 10*, 191–203.

Binaghi, E., Brivio, P. A., Ghezzi, P., & Rampini, A. (1999). A fuzzy set-based accuracy assessment of soft classification. *Pattern Recognition Letters, 20*, 935–948.

Congalton, R. G. (1991). A review of assessing the accuracy of classifications of remotely sensed data. *Remote Sensing of Environment, 37*, 35–46.

Debayle, J., & Pinoli, J. C. (2006). General adaptive neighborhood image processing. *Journal of Mathematical Imaging and Vision, 25*, 245–266.

Dehghan, H., & Ghassemian, H. (2006). Measurement of uncertainty by the entropy: application to the classification of MSS data. *International Journal of Remote Sensing, 27*, 4005–4014.

Dulyakarn, P., & Rangsanseri, Y. (2001). *Fuzzy c-means clustering using spatial information with application to remote sensing*. In: Paper presented at the 22nd Asian Conference on Remote Sensing. Vol. 5. [place unknown]; p. 9.

Foody, G. M. (2000). Estimation of sub-pixel land cover composition in the presence of untrained classes. *Computers & Geosciences, 26*, 469–478.

Geman, S., & Geman, D. (1984). Stochastic relaxation, Gibbs distributions, and the Bayesian restoration of images. *IEEE Transactions on Pattern Analysis and Machine Intelligence, PAMI-6*, 721–741.

Jackson, Q., & Landgrebe, D. A. (2002). Adaptive Bayesian contextual classification based on Markov random fields. *IEEE Transactions on Geoscience and Remote Sensing, 40*, 2454–2463.

Jensen, J. R. (1996). *Introductory digital image processing: a remote sensing perspective*. [place unknown]: Prentice-Hall Inc.

Kumar, A., Ghosh, S.K., & Dadhwal, V.K. (2006). *Sub-pixel land cover mapping: SMIC system*. ISPRS Int Sym "Geospatial Databases for Sustainable Development", Goa, India.

Li, S.Z. (1990). Reconstruction without discontinuities. In: Computer Vision, 1990 Proceedings, Third International Conference on. [place unknown]: IEEE; p. 709–712.

Li, S. Z. (1995). On discontinuity-adaptive smoothness priors in computer vision. *IEEE Transactions on Pattern Analysis and Machine Intelligence, 17*, 576–586.

Li, S. Z. (2009). *Markov random fields modeling in image analysis: e-book [Internet]. Third edition*. London: Springer. Available from: http://ezproxy.itc.nl:2048/login?url= http://dx.doi.org/10.1007/978-1-84800-279-1.

Moser, G., & Serpico, S.B. (2010). Contextual remote-sensing image classification by support vector machines and Markov random fields. Geoscience and Remote Sensing Symposium (IGARSS), 2010 I.E. International.3728–3731.

Pham, D. (2001). Spatial models for fuzzy clustering. *Computer Vision and Image Understanding, 84*, 285–297.

Solberg, A. H. S., Taxt, T., & Jain, A. K. (1996). A Markov random field model for classification of multisource satellite imagery. *IEEE Transactions on Geoscience and Remote Sensing, 34*, 100–113.

Tso, B. C. K., & Mather, P. M. (1999). Classification of multisource remote sensing imagery using a genetic algorithm and Markov random fields. *IEEE Transactions on Geoscience and Remote Sensing, 37*, 1255–1260.

Tso, B., & Mather, P. M. (2009). *Classification methods for remotely sensed data* (2nd ed.). Boca Raton: CRC.

Tso, B., & Olsen, R. C. (2005). A contextual classification scheme based on MRF model with improved parameter estimation and multiscale fuzzy line process. *Remote Sensing of Environment, 97*, 127–136.

Wen, W., & Xia, A. (1999). Verifying edges for visual inspection purposes. *Pattern Recognition Letters, 20*, 315–328.

Xu, R., & Ohya, J. (2010). An improved Kernel-based Fuzzy C-means Algorithm with spatial information for brain MR image segmentation. In: 2010 25th International Conference of Image and Vision Computing New Zealand (IVCNZ). [place unknown]; p. 1–7.

Zhang, J., & Foody, G. M. (2001). Fully-fuzzy supervised classification of sub-urban land cover from remotely sensed imagery: statistical and artificial neural network approaches. *International Journal of Remote Sensing, 22*, 615–628.